This is an open access article published under an ACS AuthorChoice License, which permits copying and redistribution of the article or any adaptations for non-commercial purposes.

THE JOURNAL OF PHYSICAL CHEMISTRY C

Article

pubs.acs.org/JPCC

# Versatile Optimization of Chemical Ordering in Bimetallic Nanoparticles

Gábor Kovács,[†] Sergey M. Kozlov,[†,§] and Konstantin M. Neyman*[,†,‡]

[†]Departament de Ciència de Materials i Química Física and Institut de Quimica Teòrica i Computacional, Universitat de Barcelona, c/Martí i Franquès 1, 08028 Barcelona, Spain

[‡]ICREA (Institució Catalana de Recerca i Estudis Avançats), Pg. Lluís Companys 23, 08010 Barcelona, Spain

**ABSTRACT:** Chemical ordering in bimetallic nanocrystallites can now be efficiently determined by density-functional calculations with the help of topological energy expressions. Herein, we deal with extending the usage of that computational scheme. We show that it enables one to structurally characterize bimetallic nanoparticles of less regular shapes than previously studied magic-type particles. In fcc Pd–Au particles of different shapes (cuboctahedral $Pd_{58}Au_{58}$, $C_{3v}$ $Pd_{61}Au_{61}$, cubic $Pd_{68}Au_{67}$, and truncated octahedral $Pd_{70}Au_{70}$), we identify the surface segregation of gold as the driving force to the lowest-energy chemical ordering. We applied the calculated descriptor values quantifying the segregation propensity of Au and energies of Pd–Au bonds in these ∼1.5 nm large particles to optimize and analyze the chemical ordering in 3.7–6 nm large Pd–Au particles. We also discuss how to predict the chemical ordering in nanoalloys at elevated temperatures. The present study paves the way to advanced structural investigations of nanoalloys to substantially accelerate their knowledge-driven engineering and manufacturing.

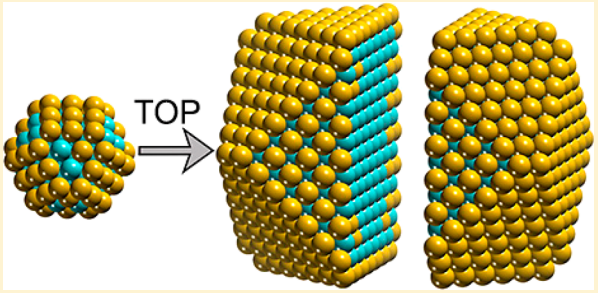


## 1. INTRODUCTION

Bimetallic nanocrystals (nanoalloys) often exhibit peculiar properties, which explains their continuously growing application in areas ranging from devices for information storage and optoelectronics to catalysis or nanomedicine.[1,2] The versatility of nanoalloys is related to their additional degrees of freedom compared to monometallic nanosystems. Indeed, varying the composition and the chemical ordering—mutual positions of different constituting metal atoms—can dramatically affect nanoalloy properties. However, these new degrees of freedom greatly increase the structural complexity of bimetallic nanomaterials making their atomic characterization very challenging. The limitation of experimental studies of nanoalloys is the lack of three-dimensional atomic resolution in common setups,[3,4] which prevents precise structural characterization of surface sites. Electronic-structure calculations do not suffer from this deficiency. However, their applications up to now have been essentially limited to investigations of relatively small heterometallic particles,[5,6] whose properties may not be representative[7,8] of the properties of larger particles dealt with in typical experiments and applications.[9,10]

Recently, we proposed a method that allows one to determine the most energetically stable atomic arrangement in several nanometer large bimetallic crystallites with a given shape and composition.[11] This topological energy expression (TOP) method enables the global optimization of mutual positions of different atoms (or chemical ordering) using calculations relying on density functional theory (DFT). According to the TOP method, the energy of a bimetallic nanoparticle (NP) $A_mB_n$ (with $m$ atoms A and $n$ atoms B) is represented as[11]

$$E_{\mathrm{TOP}} = E_0 + \varepsilon^{\mathrm{A-B}}_{\mathrm{BOND}} N^{\mathrm{A-B}}_{\mathrm{BOND}} + \varepsilon^{\mathrm{A}}_{\mathrm{CORNER}} N^{\mathrm{A}}_{\mathrm{CORNER}} + \varepsilon^{\mathrm{A}}_{\mathrm{EDGE}} N^{\mathrm{A}}_{\mathrm{EDGE}} + \varepsilon^{\mathrm{A}}_{\mathrm{TERRACE}} N^{\mathrm{A}}_{\mathrm{TERRACE}} \quad (1)$$

where $N^{\mathrm{A-B}}_{\mathrm{BOND}}$ is the number of heteroatomic bonds (nearest-neighbor pairs of atoms A and B) in the considered structure; $N^{\mathrm{A}}_{\mathrm{CORNER}}$, $N^{\mathrm{A}}_{\mathrm{EDGE}}$, and $N^{\mathrm{A}}_{\mathrm{TERRACE}}$ are the numbers of A-type atoms on corner, edge, and terrace sites, respectively; and $E_0$ is a constant for each NP shape and composition. The energetic parameters $\varepsilon_i$ in eq 1 are fitted to DFT energies of a group of NPs, called homotops,[1] i.e., species with the same shape, size, and composition but different chemical ordering. Values of $\varepsilon_i$ (denoted as descriptors herein) directly characterize the nature of binding in the considered NPs. For instance, using descriptor values, one can assess the role of surface segregation or heterometallic bond formation as the driving force for the most stable chemical ordering. The simplicity of eq 1 allows for effective identification of the global minimum using multiple exchange moves of atoms even for nanoparticles with thousands of atoms.[11]

**Special Issue:** ISSPIC XVIII: International Symposium on Small Particles and Inorganic Clusters 2016

**Received:** November 27, 2016
**Revised:** January 4, 2017
**Published:** January 5, 2017


© 2017 American Chemical Society

DOI: 10.1021/acs.jpcc.6b11923
J. Phys. Chem. C 2017, 121, 10803–10808

The TOP method was shown to successfully describe the chemical ordering in bimetallic NPs composed of different metals, such as Pt−Co,[12,13] Pt−Sn,[14] Pd−Cu,[11] Pd−Ag,[11] Pd−Au,[11] Pd−Zn,[11] and Cu−Ni.[15] However, so far the method was used to study only NPs with a highly symmetric (truncated) octahedral shape. Also, to better emulate experimental conditions in simulations, one has to account for the thermal disorder of nanoalloys at finite temperatures. We demonstrate herein that the TOP method is equally well applicable to predict structures of less symmetric bimetallic NPs equilibrated at a given temperature. We have addressed Pd−Au nanoalloys as a paradigmatic example of experimentally well studied nanoalloys[16] with numerous applications in catalysis.[17−21] In particular, recent experimental studies communicate very substantial complexity of Pd−Au nanoalloys, strong dependence of their structure on the preparation procedure and the pretreatment before using as catalysts, which result in many still debated structural questions. Because of this complexity, despite being among the best theoretically studied bimetallic particles, Pd−Au nanoalloys continue to be frequently simulated at various computational levels using the whole arsenal of models, from slabs[22,23] to subnanoscale clusters[24,25] and nanoparticles.[11,26−29] In many of these modeling studies, Pd−Au nanoalloys serve as exemplary bimetallic particles, whose accurate theoretical description requires further development and improvement of the underlined computational approaches.

Our previous analysis of truncated-octahedral *fcc* nanocrystallite $Pd_{70}Au_{70}$ revealed that the main factor that determines its most favorable chemical ordering is the segregation of Au atoms on the NP surface.[11] Moreover, for this NP shape, we showed that the less-coordinated the surface site, the more significant the energy gain for Au segregation on that particular site. The energy gain due to one Pd−Au bond formed is at least an order of magnitude less than the energy gained by surface segregation of one atom Au.[11]

## 2. COMPUTATIONAL DETAILS

Electronic structure calculations are performed using the periodic plane-wave code VASP.[30] We use the PBE[31] exchange-correlation functional, which was found to be one of the most appropriate among common functionals to describe transition metals.[32,33] The interaction between valence and core electrons was treated within the projector augmented wave approach.[34] In order to moderate the computational cost, the 250.93 eV energy cutoff of plane-wave basis sets is used (defined by the pseudopotentials of Au and Pd), since the latter cutoff value was previously shown to provide very similar energy values to more common 415 eV basis sets.[11] The one-electron levels are smeared by 0.1 eV using the first-order method of Methfessel and Paxton,[35] and the converged energies are extrapolated to the zero smearing. All calculations are performed only at the Γ-point in the reciprocal space. All atoms were allowed to relax during the geometry optimization until forces on them became less than 0.2 eV/nm. The minimal separation between NPs exceeds 0.7 nm, at which the interaction between adjacent NPs was estimated to be negligible.[36]

## 3. RESULTS AND DISCUSSION

In order to evaluate the versatility of our computational protocol, we optimized the chemical ordering in Pd−Au NPs with varied shapes. Namely, we considered the cuboctahedral $Pd_{58}Au_{58}$ particle exposing both extended {100} and {111} facets, the cubic $Pd_{68}Au_{67}$ NP, as well as $Pd_{61}Au_{61}$, whose symmetry is reduced to $C_{3v}$ (Figure 1). Table 1 lists descriptors and accuracy metrics for these NPs.

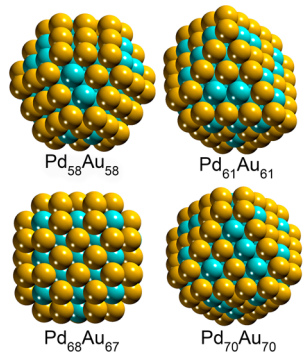


**Figure 1.** $Pd_{58}Au_{58}$, $Pd_{61}Au_{61}$, $Pd_{68}Au_{67}$, and $Pd_{70}Au_{70}$ nanoparticles with the optimized lowest-energy chemical ordering. Pd atoms - light blue, Au atoms - yellow.

**Table 1. Descriptors $\varepsilon_i$ in the Topological Energy Expressions $E_{TOP}$ for $Pd_{58}Au_{58}$, $Pd_{61}Au_{61}$, $Pd_{68}Au_{67}$, and $Pd_{70}Au_{70}$ Nanoparticles as Well as $Pd_{27}Au_{28}$ Particles along with the Corresponding Precision ($\delta$) and Accuracy ($\Delta E$) Values, all in meV[a]**

| particle | $Pd_{58}Au_{58}$ | $Pd_{61}Au_{61}$ | $Pd_{68}Au_{67}$ | $Pd_{70}Au_{70}$[b] | $Pd_{27}Au_{28}$ |
|---|---|---|---|---|---|
| $\varepsilon_{BOND}^{Pd-Au}$ | $-21^{+3}_{-3}$ | $-16^{+2}_{-3}$ | $-12^{+4}_{-3}$ | $-13^{+4}_{-6}$ | $-24^{+8}_{-7}$ |
| $\varepsilon_{CORNER}^{Au}$[c] | $-458^{+38}_{-30}$ | $-409^{+27}_{-38}$ | $-460^{+22}_{-26}$ | $-404^{+76}_{-72}$ | $-567^{+36}_{-48}$ |
| $\varepsilon_{EDGE}^{Au}$[d] | $-398^{+39}_{-69}$ | $-421^{+51}_{-35}$ | $-242^{+18}_{-14}$ | $-301^{+52}_{-77}$ | $-507^{+31}_{-54}$ |
| $\varepsilon_{TERRACE\{100\}}^{Au}$ | $-398^{+51}_{-81}$ | | $-450^{+32}_{-37}$ | | $-505^{+21}_{-30}$ |
| $\varepsilon_{TERRACE\{111\}}^{Au}$ | $-296^{+33}_{-80}$ | $-320^{+65}_{-45}$ | $-256^{+38}_{-47}$ | $-200^{+52}_{-64}$ | |
| $\delta$ | 108 | 106 | 96 | 115 | 128 |
| $\Delta E$ | 42 | 64 | 22 | 26 | 32 |
| $N$ | 51 | 27 | 45 | 32 | 40 |

[a] $N$ is the number of structures (homotops) calculated for determining the expressions $E_{TOP}$. 95% confidence intervals of $\varepsilon_i$ $\left(^{+k}_{-l}\right)$ are also shown. [b] Data from ref 11. [c] The coordination number of corner atoms in the nanoparticles is 6 except for $Pd_{61}Au_{61}$, which contains both 5- and 6-coordinated corner atoms. For the particle $Pd_{61}Au_{61}$, a common descriptor was used for all corner sites. [d] Descriptors $\varepsilon_{EDGE}^{Au}$ are for 7-coordinated edge positions in all nanoparticles except $Pd_{68}Au_{67}$, where the descriptor is used to characterize 11-coordinated subsurface edge sites. [e] $\delta$ is twice the residual standard deviation between the $E_{DFT}$ and $E_{TOP}$ energy values for a set of $N_{TEST} \geq 10$ homotops *not* included in the fitting procedure. [f] $\Delta E$ is the difference between $E_{TOP}$ of the lowest-energy homotop from the DFT calculations and of the lowest-energy homotop from the TOP optimization.

For all studied shapes of ∼1.5 nm large particles, the optimization of 30−50 structures with different chemical ordering (homotops) was enough to obtain TOP energy expressions with excellent precision $\delta \leq 115$ meV and accuracy $\Delta E \leq 64$ meV. Indeed, the precision metric evidences typical differences of less than 1 meV/atom between DFT and TOP total energies of homotops in the test set. The accuracy metric, which reflects subtle energy differences between the lowest-energy homotops obtained at DFT and TOP levels, is also remarkably strict. Irrespective of the NP shape, as a rule, the less-coordinated the surface positions, the higher the energy gain associated with Au segregation on them. Thus, the


DOI: 10.1021/acs.jpcc.6b11923
J. Phys. Chem. C 2017, 121, 10803−10808

Table 2. Number of Au Atoms on a Site with a Given Coordination Number (in Parentheses a Fraction of Such Sites Occupied by Au) in the Lowest-Energy Homotops of Different Pd−Au Particles as Well as Their Size in nm

| | size | corner | edge | {100} | {111} | interior |
|---|---|---|---|---|---|---|
| $Pd_{58}Au_{58}$ | 1.4 | 24 (100%) | 24 (100%) | 6 (100%) | 4 (17%) | 0 (0%) |
| $Pd_{61}Au_{61}$ | 1.6 | 18 (100%) | 27 (100%) | | 16 (37%) | 0 (0%) |
| $Pd_{68}Au_{67}$ | 1.5 | 48 (100%) | 0[a] (0%) | 20 (83%) | 0 (0%) | 0 (0%) |
| $Pd_{70}Au_{70}$ | 1.6 | 24 (100%) | 24 (100%) | | 22 (46%) | 0 (0%) |
| $Pd_{27}Au_{28}$ | 1.1 | 11 (92%) | 12 (50%) | 5 (83%) | | 0 (0%) |

[a]In the case of $Pd_{68}Au_{67}$, edge sites represent 11-coordinated subsurface edge positions, whereas they are 7-coordinated positions for the other studied NPs.

segregation energy of Au is more substantial for low-coordinated corner and edge sites than for either {100} or {111} terrace positions.

Close similarities in the respective descriptor values also clearly manifest in the most stable chemical orderings for the different NP shapes at 0 K (Figure 1, Table 2). For all of these shapes, 100% of Au atoms reside on the NP surface, whereas the interior consists of Pd.

In the lowest-energy homotop of cuboctahedral $Pd_{58}Au_{58}$, gold atoms occupy all 6-coordinated corner and 7-coordinated edges together with all 8-coordinated {100} terrace sites. The remaining gold atoms are in 9-coordinated {111} terrace positions. There are two types of corner positions (5- and 6-coordinated ones) in the $C_{3v}$ $Pd_{61}Au_{61}$ NP, all occupied by gold in the lowest-energy structure. Similarly, 7-coordinated edges there are also fully occupied by Au atoms, whereas the remaining gold atoms are situated on 9-coordinated {111} terraces. In the most stable homotop of cubic $Pd_{68}Au_{67}$, gold atoms occupy all 6-coordinated corner sites, whereas the rest of the gold is in 9-coordinated {111} terrace positions. The lowest-energy structure of truncated octahedral $Pd_{70}Au_{70}$ NP shows similar features;[11] that is, low-coordinated corner and edge sites are fully occupied by gold atoms, whereas the rest of the gold is located at {111} terraces.

On the basis of the descriptors in Table 1 and the structure of the lowest-energy homotops for each NP (Figure 1, Table 2), we can conclude that, independently of the shape of the studied NPs, gold, in general, prefers less-coordinated surface sites. The preference of gold follows the order corner > edge > {100} terrace > {111} terrace positions. Note that in $Pd_{68}Au_{67}$ the atoms denoted as "edges" are in fact 11-coordinated subsurface edges. Hence, it is not surprising that Au atoms do not tend to occupy these positions.

The original methodology[11] allowed one to obtain homotops with the most energetically stable chemical ordering (discussed above), which correspond to the ground-state species to be observed experimentally at very low temperatures. To deal with nanoparticle models representative of experimental structures at higher temperatures, we modified the computational protocol in order to estimate properties associated with the Boltzmann population of different homotops for a given NP. For instance, the aforementioned analysis lets us determine average structural NP properties at elevated temperatures, which is essential for predicting the chemical (dis-)ordering in NPs in different applications. Note, however, that this method accounts only for degrees of freedom associated with chemical ordering but not with atomic vibrations. Note also that the simplicity of eq 1 allows one to obtain well-converged thermodynamic values averaged over up to billions of Monte Carlo steps.

To demonstrate the potential of the methodology, we calculated the average chemical ordering for the previously introduced Pd−Au NPs in a temperature range of 0−1000 K. In accordance with the Metropolis algorithm, the averaging was done over accepted configurations, whose statistical weights were proportional to the number of rejected moves from each of these configurations. As a result, we were able to determine the probability of occupation of each site by either Au or Pd. For instance, it can be seen that, whereas at 0 K all Au atoms are situated at the NP surface, the concentration of Au atoms in the interior gradually increases up to 10−15% at 1000 K, depending on the NP shape (Figure 2).

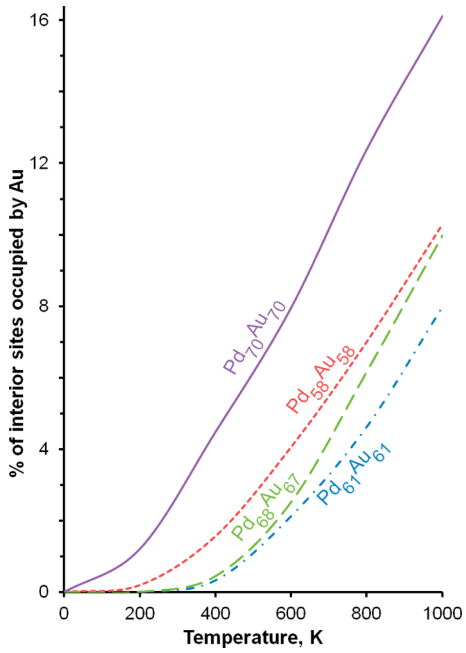


Figure 2. Equilibrium concentration of Au atoms in the interior of Pd−Au nanoparticles as a function of temperature. Interior atoms are those not exposed on the nanoparticle surface.

Obviously, the TOP method is not designed to reliably optimize the chemical ordering in small bimetallic clusters, which may exhibit substantial distortions from the crystalline lattice atomic positions. However, it is important to evaluate the applicability of this computational methodology for the description of bimetallic particles at sizes around 1 nm. We explored the performance of the TOP approach by optimizing the chemical ordering in a truncated-octahedral $Pd_{27}Au_{28}$ particle with the dimension of 1.1 nm.

Analysis of the calculated data (see Table 1) reveals that the present methodology can also reliably predict the chemical



DOI: 10.1021/acs.jpcc.6b11923
J. Phys. Chem. C 2017, 121, 10803−10808

ordering in $Pd_{27}Au_{28}$ with good accuracy ($\delta$ = 128 meV) and precision ($\Delta E$ = 32 meV). The qualitative results obtained for $Pd_{27}Au_{28}$ are similar to those presented in Table 1 for larger particles. The key factor of the optimal chemical ordering in $Pd_{27}Au_{28}$ is also the surface segregation of gold atoms. The heteroatomic bond formation is slightly exothermic, by 24 meV, like for larger studied Pd−Au particles. The surface segregation energies of Au atoms are −567 meV for 5-coordinated corners, −507 meV for 7-coordinated edge sites, and −505 meV for 8-coordinated {100} terrace sites. These values are somewhat larger in magnitude than those for all other particles in Table 1. The segregation propensity of gold is the strongest for corner positions, whereas segregation on edges or terrace sites is characterized by essentially the same energy. This is also reflected in the structural arrangement of the lowest-energy $Pd_{27}Au_{28}$ homotop: there all but one corner positions are occupied by gold, whereas the remaining gold atoms are distributed between 7-coordinated edge and 8-coordinated terrace sites (Table 2, Figure 3).

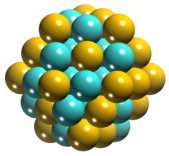

**Figure 3.** $Pd_{27}Au_{28}$ particle with optimized chemical ordering. Pd atoms - light blue, Au atoms - yellow.

One can also apply the descriptors fitted to energies of ∼1.5 nm large Pd−Au particles to optimization of much larger species, which are often encountered in experiments and applications. Such extrapolation is possible, since descriptors were shown not to depend significantly on the particle size for NPs > 1.2 nm.[11,12] Namely, we optimized the chemical ordering in 3.7−4.4 nm large particles of 1264−1603 atoms and 5.4−6.0 nm large particles of 2764−3630 atoms with different shapes using the respective descriptors from Table 1.

Due to the varying NP shape among the considered species, there is a significant variation of the surface-to-interior ratio and of the abundance of particular sites on the nanoparticle surface. Nevertheless, the amount of Au atoms in these NPs is sufficient to fully populate all available surface sites (Figure 4, Table 3). The difference in the composition of the considered Pd−Au particles is limited to the concentration of Au in the nanoparticle interior. In 1:1 Pd−Au particles of 3.7−4.4 nm, the concentration of Au in the NP interior varies from 16% in the $C_{3v}$ $Pd_{632}Au_{632}$ particle with the highest surface-to-interior ratio to 22% in the more compact cubic $Pd_{802}Au_{801}$ and cuboctahedral $Pd_{644}Au_{644}$ NPs. The variation is smaller in 5.4−6.0 nm large particles, from 27% of Au in the interior of the octahedral $Pd_{1638}Au_{1637}$ to 32% in cuboctahedral $Pd_{1815}Au_{1815}$. Although the Au concentration in the NP interior increases with the particle size, it is still significantly below 50% even in 6.0 nm large 1:1 Pd−Au particles.

One of the central points of this investigation is that neither the descriptors related to the surface segregation of Au nor the descriptor of Pd−Au bonds vary in a significant manner among NPs of different shapes (Table 1). Hence, factors governing the most energetically stable chemical ordering in Pd−Au nanoalloys are as weakly dependent on the NP shape as they were shown to be on the NP size.[11,12]

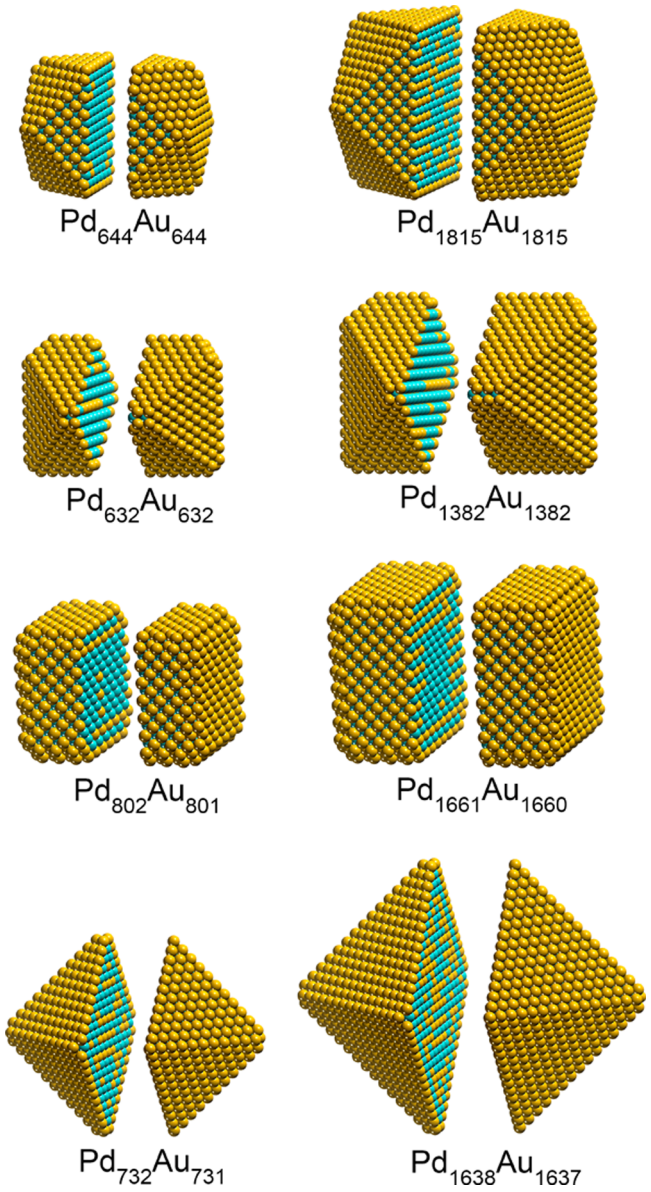


**Figure 4.** Lowest-energy chemical ordering of larger Pd−Au nanoparticles split in halves. Pd atoms - light blue, Au atoms - yellow.

In order to rigorously show the implications of this result, we took descriptors optimized for the cuboctahedral $Pd_{58}Au_{58}$ nanoparticle and used them to calculate the energetically most favorable chemical ordering in octahedral $Pd_{70}Au_{70}$ and $C_{3v}$ $Pd_{61}Au_{61}$ particles as well as in the respective larger octahedral $Pd_{732}Au_{731}$ and $C_{3v}$ $Pd_{632}Au_{632}$ species. We could not perform such an analysis for cubic $Pd_{68}Au_{67}$ and $Pd_{802}Au_{801}$, since the latter contains 11-coordinated subsurface edge atoms absent in $Pd_{58}Au_{58}$. We found that the lowest-energy structures of the analyzed octahedral and $C_{3v}$ particles were completely identical (i.e., had the same parameters as given in Tables 2 and 3) whether we used the descriptors fitted for the respective shapes or for the cuboctahedral $Pd_{58}Au_{58}$. This finding evidences that the differences between the descriptors for Pd−Au nanoparticles with the same composition but different shapes (Table 1) are really minor, since such differences do not alter the driving forces causing the most stable chemical ordering in the NPs.



DOI: 10.1021/acs.jpcc.6b11923
J. Phys. Chem. C 2017, 121, 10803−10808

Table 3. Number of Au Atoms on a Site with a Given Coordination Number (in Parentheses a Fraction of Such Sites Occupied by Au) in the Lowest-Energy Homotops of Large Pd−Au Nanoparticles as Well as Their Size in nm

| | size | corner | edge | {100} | {111} | interior |
|---|---|---|---|---|---|---|
| CO-$Pd_{644}Au_{644}$ | 3.7 | 24 (100%) | 120 (100%) | 150 (100%) | 168 (100%) | 192 (22%) |
| CO-$Pd_{1815}Au_{1815}$ | 5.4 | 24 (100%) | 192 (100%) | 384 (100%) | 360 (100%) | 855 (32%) |
| $C_{3v}$-$Pd_{632}Au_{632}$ | 4.1 | 24 (100%) | 102 (100%) | | 388 (100%) | 118 (16%) |
| $C_{3v}$-$Pd_{1382}Au_{1382}$ | 5.4 | | | | | |
| C-$Pd_{802}Au_{801}$ | 4.2 | | 144[a] (100%) | 360 (100%) | 8 (100%) | 229 (22%) |
| C-$Pd_{1661}Au_{1660}$ | 5.5 | | 192[a] (100%) | 672 (100%) | 8 (100%) | 704 (30%) |
| O-$Pd_{732}Au_{731}$ | 4.4 | 24 (100%) | 108 (100%) | | 440 (100%) | 159 (18%) |
| O-$Pd_{1638}Au_{1637}$ | 6.0 | 24 (100%) | 156 (100%) | | 840 (100%) | 617 (27%) |

[a]Edges of $Pd_{802}Au_{801}$ and $Pd_{1661}Au_{1660}$ nanoparticles are composed of 6-coordinated atoms (values in the table) as well as 11-coordinated sites. The latter sites are fully occupied by 60 and 84 Au atoms, respectively.

## 4. CONCLUSIONS

We have demonstrated that the new TOP method for the optimization of the chemical ordering in bimetallic nanoparticles is applicable equally efficiently and accurately to high- and low-symmetry particles. We showed that, independently of the particle shape, the key factor in the optimal chemical ordering in Pd−Au nanoparticles with >100 atoms is the propensity of gold atoms to segregate on the surface. Moreover, for any of the shapes under scrutiny, the energy gain from the surface segregation of gold becomes greater or equal, when the surface segregated atom is less coordinated. The segregation energies for a particular type of site vary insignificantly between the considered 1:1 Pd−Au nanoparticles, which is demonstrated by the transferability of the segregation descriptors across particles of different shapes for the purpose of structural optimization.

The TOP methodology accurately describes the chemical ordering also in twice smaller particles, such as $Pd_{27}Au_{28}$, being at the borderline between molecular clusters and metallic nanoparticles. Notably, for $Pd_{27}Au_{28}$ species, the descriptors are found to be larger in magnitude than for larger particles, thus reflecting the non-negligible size dependence of the chemical interactions in smaller bimetallic particles when they acquire molecular properties.

The noticed presence of Pd on the surface of the lowest-energy homotops of 1:1 Pd-Au nanoparticles smaller than 2 nm and the absence of Au in their interior is assigned to an insufficient amount of Au to fully cover the nanoparticle surface. However, Au is able to cover the whole surface of nanoparticles consisting of more than 1200 atoms. There, the concentration of Au in the NP interior becomes noticeable, although it remains significantly below 50% even for the largest calculated particle of 3630 atoms.

We have shown that our computational method can now provide average properties of bimetallic nanoparticles at moderately elevated temperatures and thus more adequately simulate their chemical ordering in typical experimental situations.

The results outlined above show that the TOP method with its recent implementations can play the role of a very efficient and versatile computational tool for determining the atomic arrangement in bimetallic particles with different combinations of metals and a wide range of sizes, shapes, and compositions. As a caveat, we mention that significant deviations from the uniform alloy lattice, e.g., due to the large size mismatch of the constituting metal atoms, are expected to limit application of the TOP method. The latter, however, has not been the case for a variety of bimetallic nanoparticles studied using this method to date.[11−15] The method provides invaluable data on atomic arrangements in nanoalloys, which are mandatory for rapid manufacturing of advanced bimetallic nanomaterials via their knowledge-driven design.

## AUTHOR INFORMATION


### Corresponding Author

*E-mail: konstantin.neyman@icrea.cat.

### ORCID

Konstantin M. Neyman: 0000-0002-5242-5567

### Present Address

[§]S.M.K.: KAUST Catalysis Research Center, Physical Sciences and Engineering Division, King Abdullah University of Science and Technology, Thuwal 23955-6900, Kingdom of Saudi Arabia.


### Notes

The authors declare no competing financial interest.

## ACKNOWLEDGMENTS

This study was supported by the European Commission (FP7-NMP.2012.1.1-1 project ChipCAT, ref. 310191), the Spanish MINECO (grants CTQ2012-34969, CTQ2015-64618-R with FEDER), and the Generalitat de Catalunya (projects 2014SGR97 and XRQTC). The authors thank the Red Española de Supercomputación for the computer resources at *MEMENTO* and the technical support provided by *CAESARAUGUSTA* (QCM-2015-1-0025, QCM-2015-2-0016).

## REFERENCES


(1) Ferrando, R.; Jellinek, J.; Johnston, R. L. Nanoalloys: From Theory to Applications of Alloy Clusters and Nanoparticles. *Chem. Rev.* **2008**, *108*, 845−910.

(2) Calvo, F., Ed. *Nanoalloys: From Fundamentals to Emergent Applications*; Elsevier: Amsterdam, The Netherlands, 2013.

(3) Gan, L.; Cui, C.; Heggen, M.; Dionigi, F.; Rudi, S.; Strasser, P. Element-Specific Anisotropic Growth of Shaped Platinum Alloy Nanocrystals. *Science* **2014**, *346*, 1502−1506.

(4) Tan, X.; Prabhudev, S.; Kohandehghan, A.; Karpuzov, D.; Botton, G. A.; Mitlin, D. Pt−Au−Co Alloy Electrocatalysts Demonstrating Enhanced Activity and Durability toward the Oxygen Reduction Reaction. *ACS Catal.* **2015**, *5*, 1513−1524.

(5) Tan, T. L.; Wang, L. L.; Johnson, D. D.; Bai, K. A Comprehensive Search for Stable Pt−Pd Nanoalloy Configurations and Their Use as Tunable Catalysts. *Nano Lett.* **2012**, *12*, 4875−4880.

(6) Schebarchov, D.; Wales, D. J. Structure Prediction for Multicomponent Materials Using Biminima. *Phys. Rev. Lett.* **2014**, *113*, 156102.




DOI: 10.1021/acs.jpcc.6b11923
J. Phys. Chem. C 2017, 121, 10803−10808

(7) Kaden, W. E.; Wu, T.; Kunkel, W. A.; Anderson, S. L. Electronic Structure Controls Reactivity of Size-Selected Pd Clusters Adsorbed on $TiO_2$ Surfaces. *Science* **2009**, *326*, 826−829.
(8) Yudanov, I. V.; Genest, A.; Schauermann, S.; Freund, H.-J.; Rösch, N. Size Dependence of the Adsorption Energy of CO on Metal Nanoparticles: A DFT Search for the Minimum Value. *Nano Lett.* **2012**, *12*, 2134−2139.
(9) Molenbroek, A. M.; Helveg, S.; Topsøe, H.; Clausen, B. S. Nano-Particles in Heterogeneous Catalysis. *Top. Catal.* **2009**, *52*, 1303−1311.
(10) Roldan Cuenya, B.; Behafarid, F. Nanocatalysis: Size- and Shape-Dependent Chemisorption and Catalytic Reactivity. *Surf. Sci. Rep.* **2015**, *70*, 135−187.
(11) Kozlov, S. M.; Kovács, G.; Ferrando, R.; Neyman, K. M. How to Determine Accurate Chemical Ordering in Several Nanometer Large Bimetallic Crystallites from Electronic Structure Calculations. *Chem. Sci.* **2015**, *6*, 3868−3880.
(12) Kovács, G.; Kozlov, S. M.; Matolínová, I.; Vorokhta, M.; Matolín, V.; Neyman, K. M. Revealing Chemical Ordering in Pt-Co Nanoparticles Using Electronic Structure Calculations and X-Ray Photoelectron Spectroscopy. *Phys. Chem. Chem. Phys.* **2015**, *17*, 28298−28310.
(13) Vorokhta, M.; Khalakhan, I.; Václavů, M.; Kovács, G.; Kozlov, S. M.; Kúš, P.; Skála, T.; Tsud, N.; Lavková, J.; Potin, V.; et al. Surface Composition of Magnetron Sputtered Pt-Co Thin Film Catalyst for Proton Exchange Membrane Fuel Cells. *Appl. Surf. Sci.* **2016**, *365*, 245−251.
(14) Neitzel, A.; Kovács, G.; Lykhach, Y.; Kozlov, S. M.; Tsud, N.; Skála, T.; Vorokhta, M.; Matolín, V.; Neyman, K. M.; Libuda, J. Atomic Ordering and Sn Segregation in Pt-Sn Nanoalloys Supported on $CeO_2$ thin films. *Top. Catal.* **2016**, DOI: 10.1007/s11244-016-0709-5.
(15) Wolfbeisser, A.; Kovács, G.; Kozlov, S. M.; Föttinger, K.; Bernardi, J.; Klötzer, B.; Neyman, K. M.; Rupprechter, G. Surface Composition Changes of CuNi-$ZrO_2$ During Methane Decomposition: An *Operando* NAP-XPS and Density Functional Study. *Catal. Today* **2017**, *283*, 134−143.
(16) Hutchings, G. J.; Kiely, C. J. Strategies for the Synthesis of Supported Gold Palladium Nanoparticles with Controlled Morphology and Composition. *Acc. Chem. Res.* **2013**, *46*, 1759−1772.
(17) Edwards, J. K.; Solsona, B.; Carley, A. F.; Herzing, A. A.; Kiely, C. J.; N, E. N.; Hutchings, G. J. Switching Off Hydrogen Peroxide Hydrogenation in the Direct Synthesis Process. *Science* **2009**, *323*, 1037−1041.
(18) Dhital, R. N.; Kamonsatikul, C.; Somssok, E.; Bobuatong, K.; Ehara, M.; Karanjit, S.; Sakurai, H. Low-Temperature Carbon−Chlorine Bond Activation by Bimetallic Gold/Palladium Alloy Nanoclusters: An Application to Ullmann Coupling. *J. Am. Chem. Soc.* **2012**, *134*, 20250−20253.
(19) Nie, M.; Shen, P. K.; Wei, Z. Nanocrystaline Tungsten Carbide Supported Au−Pd Electrocatalyst for Oxygen Reduction. *J. Power Sources* **2007**, *167*, 69−73.
(20) Bulushev, D. A.; Beloshapkin, S.; Plyusnin, P. E.; Shubin, Y. V.; Bukhtiyarov, V. I.; Korenev, S. V.; Ross, J. R. H. Vapour Phase Formic Acid Decomposition over PdAu/$\gamma$-$Al_2O_3$ Catalysts: Effect of Composition of Metallic Particles. *J. Catal.* **2013**, *299*, 171−180.
(21) Kolli, N. E.; Delannoy, L.; Louis, C. Bimetallic Au−Pd Catalysts for Selective Hydrogenation of Butadiene: Influence of the Preparation Method on Catalytic Properties. *J. Catal.* **2013**, *297*, 79−92.
(22) Yu, W.-Y.; Zhang, L.; Mullen, G. M.; Evans, E. J., Jr.; Henkelman, G.; Mullins, C. B. Effect of Annealing in Oxygen on Alloy Structures of Pd−Au Bimetallic Model Catalysts. *Phys. Chem. Chem. Phys.* **2015**, *17*, 20588−20596.
(23) Creuze, J.; Guesmi, H.; Mottet, C.; Zhu, B.; Legrand, B. Surface Segregation in AuPd Alloys: Ab initio Analysis of the Driving Forces. *Surf. Sci.* **2015**, *639*, 48−53.
(24) Shayeghi, A.; Götz, D.; Davis, J. B. A.; Schäfer, R.; Johnston, R. L. Pool-BCGA: A Parallelised Generation-Free Genetic Algorithm for the *ab initio* Global Optimisation of Nanoalloy Clusters. *Phys. Chem. Chem. Phys.* **2015**, *17*, 2104−2112.
(25) Hussein, H. A.; Davis, J. B. A.; Johnston, R. L. DFT Global Optimisation of Gas-Phase and MgO-Supported Sub-Nanometre AuPd Clusters. *Phys. Chem. Chem. Phys.* **2016**, *18*, 26133−26143.
(26) Yudanov, I. V.; Neyman, K. M. Stabilization of Au at Edges of Bimetallic PdAu Nanocrystallites. *Phys. Chem. Chem. Phys.* **2010**, *12*, 5094−5100.
(27) Marchal, R.; Genest, A.; Krüger, S.; Rösch, N. Structure of Pd/Au Alloy Nanoparticles from a Density Functional Theory-Based Embedded-Atom Potential. *J. Phys. Chem. C* **2013**, *117*, 21810−21822.
(28) Spitale, A.; Perez, M. A.; Mejía-Rosales, S.; Yacamán, M. J.; Mariscal, M. M. Gold-Palladium Core@Shell Nanoalloys: Experiments and Simulations. *Phys. Chem. Chem. Phys.* **2015**, *17*, 28060−28067.
(29) Zhu, B.; Guesmi, H.; Creuze, J.; Legrand, B.; Mottet, C. Crossover among Structural Motifs in Pd−Au Nanoalloys. *Phys. Chem. Chem. Phys.* **2015**, *17*, 28129−28136.
(30) Kresse, G.; Furthmuller, J. Efficient Iterative Schemes for *ab initio* Total-Energy Calculations Using a Plane-Wave Basis Set. *Phys. Rev. B: Condens. Matter Mater. Phys.* **1996**, *54*, 11169−11186.
(31) Perdew, J. P.; Burke, K.; Ernzerhof, M. Generalized Gradient Approximation Made Simple. *Phys. Rev. Lett.* **1996**, *77*, 3865−3868.
(32) Janthon, P.; Kozlov, S. M.; Viñes, F.; Limtrakul, J.; Illas, F. Establishing the Accuracy of Broadly Used Density Functionals in Describing Bulk Properties of Transition Metals. *J. Chem. Theory Comput.* **2013**, *9*, 1631−1640.
(33) Janthon, P.; Luo, S.; Kozlov, S. M.; Viñes, F.; Limtrakul, J.; Truhlar, D. G.; Illas, F. Bulk Properties of Transition Metals: A Challenge for the Design of Universal Density Functionals. *J. Chem. Theory Comput.* **2014**, *10*, 3832−3839.
(34) Kresse, G.; Joubert, D. From Ultrasoft Pseudopotentials to the Projector Augmented-Wave Method. *Phys. Rev. B: Condens. Matter Mater. Phys.* **1999**, *59*, 1758−1775.
(35) Methfessel, M.; Paxton, A. T. High-Precision Sampling for Brillouin-Zone Integration in Metals. *Phys. Rev. B: Condens. Matter Mater. Phys.* **1989**, *40*, 3616−3621.
(36) Viñes, F.; Illas, F.; Neyman, K. M. On the Mechanism of Formation of Metal Nanowires by Self-Assembly. *Angew. Chem., Int. Ed.* **2007**, *46*, 7094−7097.


DOI: 10.1021/acs.jpcc.6b11923
*J. Phys. Chem. C* 2017, 121, 10803−10808